POLITECNICO
MILANO 1863

SCUOLA DI INGEGNERIA INDUSTRIALE
E DELL'INFORMAZIONE

EXECUTIVE SUMMARY OF THE THESIS

# Development of a test protocol for the mechanical analysis of custom-made sub-periosteal dental implants: numerical – experimental integrated approach

TESI MAGISTRALE IN BIOMEDICAL ENGINEERING – INGEGNERIA BIOMEDICA

**AUTHOR: GIACOMO NEGRINI**

**ADVISOR: PROF. DARIO GASTALDI**

**CO-ADVISOR: ING. ILARIA ROTA, ING. LUCA CIRIELLO**

**ACADEMIC YEAR: 2020-2021**

## 1. Introduction

To date, 90% of global population have had, at least once in their life, oral diseases. These include soft tissues and hard tissues diseases, like caries, periodontal disease, oral cancer, and mandibular/maxillary atrophies. Among these, bone cancer and bone atrophies represent the worst-case scenarios. These clinical cases, indeed, cause tooth loss due to the surgical removal or the resorption of a portion of bone, respectively [1, 2, 3]. Typically, edentulous patients are treated with endosseous implants. However, in case of severe resorption (Class V and Class VI of the Cawood and Howell's classification), patients can't be treated with endosseous implants due to the absence of enough bone tissue where to insert the implant itself [4]. For this reason, thanks to the improvement of acquisition and production technologies, subperiosteal implants are more and more used. This implant is a custom-made device realized ad-hoc for the patient. Starting from CT acquisitions of the patient's residual maxillary or mandibular bone, the shape and structure of the implant is designed to perfectly wrap the bone tissue. Then, starting from the CAD file, the implant is manufactured layer by layer thanks to Additive Manufacturing techniques. To date, there are no standards to follow to test mechanical properties of subperiosteal implant. For this reason, there are no criteria to declare them safe and effective once implanted in vivo. This thesis project aims to develop an experimental setup used to mechanically test different subperiosteal implants. Then, reproducing the same loading and constraint conditions, a finite element model of the setup is realized. Once validated, this computational model will be able to verify the mechanical resistance of any type and shape of new subperiosteal implants, reducing costs and time typically associated to experimental tests. For this purpose, two different experimental setups, mandibular and maxillary, respectively, were designed and realized. Each setup was initially

tested *in vitro* and then *in silico*. To validate the computational model, the goal was to reproduce, as best as possible, the experimental Force – Displacement curves obtained after *in vitro* compression tests.

## 2. Material and Methods

For this thesis work, a mandibular and a maxillary subperiosteal implant, as well as all the designed setup components, were manufactured by Ars&Technology S.r.l. (Figure 1).

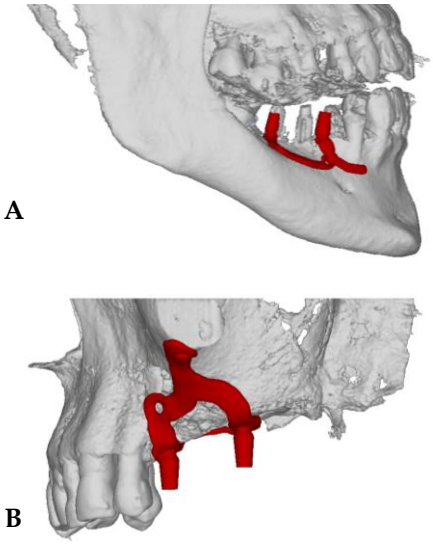


Figure 1: Lateral views of two subperiosteal implants: A) Mandibular implant; B) Maxillary implant.

### 2.1. Experimental Setup

The experimental setup was designed starting from CT images taken from the patient. For each clinical case, the bone surrounding the implant was isolated. Then, artifact associated to the CT acquisition and the trabecular structure of the bone tissue were manually cleaned and removed using MeshLab® software. To proper load and constrain the whole setup, polymeric bone phantoms and several auxiliary components were designed and realized using Solidworks® software:

- Implant

To avoid the development of any concentrated force during the compression test, the extremity of each abutment was modified. Therefore, to better accommodate the load distribution, hemispheric caps were designed to guarantee a simultaneous application of the load on the two abutments (Figure 2). Both implants have been manufactured with Ti-6Al-4V ELI titanium alloy, using Laser Powder Bed Fusion (LPBF) technique.

Figure 2: Mandibular subperiosteal implant with two hemispheric caps on the abutments.

- Bone phantom

To allow a perfect coupling with the associated implant, the superior surface of the bone has been left unaltered. Inferior portion, instead, was modified to guarantee proper support and constraint during tests. This component has been realized with a polymeric resin using 3D printing (Figure 3).

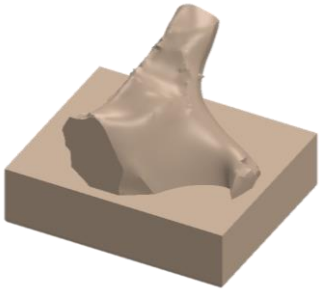

Figure 3: Maxillary bone phantom.

- Container

This element was produced to lock any possible movement and rotation of the setup during tests. During in vitro tests, the inferior extrusion of this component is grabbed by the testing machine jaws avoiding any possible resin fracture. This component was realized in Peraluman, a particular aluminum alloy.

- Spacers

Three types of spacers are designed to be placed over each hemispheric abutment giving the system the possibility to settle during the loading phase. Moreover, to cope possible setup misalignments, each component was produced with five different heights.

- Superior Plate

This component is designed with a proper length to lean on both spacers and has the function to transfer and split loads along the two abutments. To contain the spherical punch used to load the

entire setup, a conical flare was realized on the superior surface.

The overall setup was designed to have the axis of the solicitation punch aligned with the axis of the load cell, placed in the base of the test machine (Figure 4).

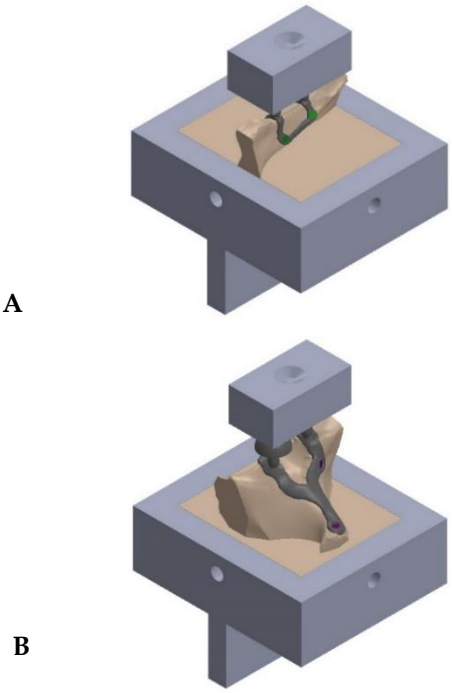


Figure 4: Representation of both experimental setups: A) Mandibular implant; B) Maxillary implant.

## 2.2. Resin characterization

To better reproduce each experimental setup *in silico*, the characterization of the mechanical properties of the resin was performed. To understand the role and the behavior of this material, two different analyses were conducted: compression test and nano-indentation test. For these analyses, 5 cubical and 5 cylindrical samples were produced by Ars&Technology S.r.l.

- Compression analysis

Three cylindrical samples were compressed (MTS 858 Mini Bionix test machine) with a speed of 0.01 mm/s until a maximum force of 3000 N was registered. To obtain the real stiffness of each polymeric sample, the resulted Force – Displacement experimental curves were filtered and corrected using Matlab®. Knowing the stiffness and the size of the samples, the Young modulus associated to the initial linear elastic response of the material was computed as:

$$E_{sample} = \frac{K_{sample} \cdot l_{sample}}{A_{sample}} \qquad 2.1$$

Where $E_{sample}$ is the elastic modulus of the resin, $K_{sample}$ is the stiffness of the resin, $l_{sample}$ is the length of the sample and $A_{sample}$ is the cross-section area of the sample. This test was compared with a finite element analysis of the same setup. This analysis was used to define a range of possible Poisson's coefficient and the elastoplastic behavior of this material. To understand which combination of Poisson coefficient of the resin and friction coefficient between cylinder and compression plates best fits the experimental results, several simulations were executed combining different values for each parameter.

- Nano-indentation analysis

To penetrate the surface of the resin, a Berkovich diamond tip was used (Nanotest Platform 3). From the analysis of the Force – Penetration experimental curve, the value of the reduced modulus ($E^*$) was computed. This value, according to the Poisson coefficient defined in the previous test, is converted in the real elastic modulus using the following equation [5]:

$$\frac{1}{E^*} = \frac{1-\nu_d^2}{E_d} + \frac{1-\nu^2}{E} \qquad 2.2$$

Where $E^*$ is the reduced modulus obtained from the indentation, $E_d$ is the diamond's elastic modulus (1141 GPa), $\nu_d$ is the diamond's Poisson coefficient (0.07), $E$ is the elastic modulus of the resin and $\nu$ is the Poisson coefficient of the resin. This analysis was performed at first on the external surface of the cubical samples, varying the applied load and creep period (Table 1).

| | Load [mN] | | | Creep [s] | | |
|---|---|---|---|---|---|---|
| **Case 1** | 200 | | | 30 | 60 | 90 |
| **Case 2** | 200 | 300 | 400 | 60 | | |

Table 1: Nano-indentation tests on the external surface of the resin.

Then, the analysis focused on the internal cross section of two cylindrical samples, virgin and already compressed, respectively. This last evaluation was used to understand if there was a significant evidence of the curing post-production process on the mechanical properties of this material. In fact, indenting along radial direction, it was possible to assess how relevant was the variation of properties. To verify if the properties

in the bulk and on the border were statistically different, the Mann-Whitney U Test was used.

## 2.3. Experimental tests

Once assembled all the elements, each setup was subjected to compression, using MTS 858 Mini Bionix test machine. A controlled displacement (0.02 mm/s) was imposed to the whole setup until the registered force reached a maximum imposed limit. There were conducted four tests whose maximum force limit was set at 200 N, 500 N, 750 N and 1000 N, respectively. For each test, 5 loading – unloading cycles were executed. The first one was used to assemble all the upper components and was not considered in the results analysis. The remaining cycles were conducted with a loading phase reaching the maximum force and an unloading phase until a lower limit of 10 N. From these tests, Force – Displacement experimental curves were obtained. Each curve was filtrated from the acquisition noise, using Matlab®, and then corrected to remove the compliance associated to the test machine. This operation was crucial to understand the real stiffness of each setup.

## 2.4. *In silico* tests

To perform a finite element analysis, the mandibular and maxillary setups were reproduced with Abaqus® software. While *in vitro* implants were already fixated to their bone phantoms, during *in silico* analysis it was necessary to realize screws to guarantee a proper interaction between implants and resin bone phantoms.

- Material assignation

Mechanical properties of each component were implemented in the software. Implants and spacers were produced in Ti-6Al-4V ELI (E = 107007 MPa, $\nu$ = 0.34), screws were produced in Ti-6Al-4V Grade 5 (E = 114000 MPa, $\nu$ = 0.33), container and superior plate were made of Peraluman (E = 69800 MPa, $\nu$ = 0.3). Properties of the polymeric resin are obtained from *in vitro* characterization.

- Interactions

The interaction between each couple of materials is characterized by its own friction coefficient (F.C.). Several couplings were defined: Peraluman – Resin (F.C. = 0.5), Ti-6Al-4V ELI – Resin (F.C. = 0.9), Peraluman – Ti-6Al-4V ELI (F.C. = 0.01), Ti-6Al-4V ELI – Ti-6Al-4V ELI (F.C. = 0.45), Ti-6Al-4V Grade 5 – Ti-6Al-4V ELI (F.C. = 0.45). The presence of the screws inside the bone component was reproduced with a "*Tie Contact*" constraint between screws and bone itself. Then, to properly transfer loads to the whole setup, a "*Coupling*" constraint was imposed between a *Reference Point*, defined in the apex of the overall setup, and the flare of the superior plate.

- Loads and constraint

In the computational analysis, the locking constraint was imposed to the inferior extrusion of the container. Then, the force generated by the tightening moment, applied during the insertion of the screws in the bone phantom, was realized with "Bolt Load". The applied force, for each screw, was obtained from the following equations:

$$M_s = V \cdot \left[ f_1 \frac{D_m}{2} + \frac{d_m}{2} tg(\varphi' + \alpha) \right] \qquad 2.2$$

$$\varphi' = arctg\left(\frac{f_2}{\cos\theta}\right) \qquad 2.3$$

$$\alpha = arctg\left(\frac{p}{\pi\, d_m}\right) \qquad 2.4$$

Where $M_s$ is the tightening moment applied to the screw, $V$ is the force generated in the screw, $f_1$ is the friction coefficient between screws and implant, $D_m$ is the screw's head mean diameter (≅ 1.5 d), $d$ is the diameter of screw stem, $d_m$ is the mean screw diameter (≅ 0.9 d), $f_2$ is the friction coefficient between screws and bone phantoms, $\theta$ is the half thread angle and $p$ is the thread pitch. Finally, downward displacement of 0.4 mm is imposed to the *Reference Point* defined in the apex of the setup.

- Mesh generation

Each component had been discretize using finite elements. For each experimental setup, implants and bone phantoms were discretized with quadratic tetrahedral elements with modified formulation (C3D10M) while other auxiliary components were discretized with linear tetrahedral elements (C3D4).

# 3. Results

## 3.1. Resin characterization

- Compression analysis

From *in vitro* analysis of the polymeric resin samples, a mean stiffness of 2685.7 N/mm and a

mean elastic modulus of 874.1 MPa were computed. From *in silico* analysis of the same setup, suitable values of the Poisson coefficient for the resin were found to belong to the range [0.25; 0.35]. Moreover, the elastoplastic behavior of the polymeric resin was obtained. Figure 5 shows the comparison between *in vitro* and *in silico* Force – Displacement curves obtained from the compression of cylindrical samples.

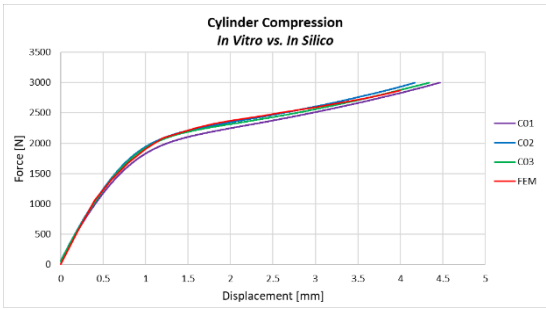


Figure 5: Comparison between *in vitro* and *in silico* Force – Displacement curves. Numerical analysis was performed with Poisson coefficient equal to 0.35

- Nano-indentation analysis

The analysis performed on the external surface of the resin showed that, for the same applied load, the elastic modulus decreased increasing the creep period. Instead, keeping fixated the creep time, increasing the applied load leads to an increased elastic modulus. The analysis performed on the cross section of the cylindrical samples showed a variation of the mechanical properties along radial direction (Figure 6).

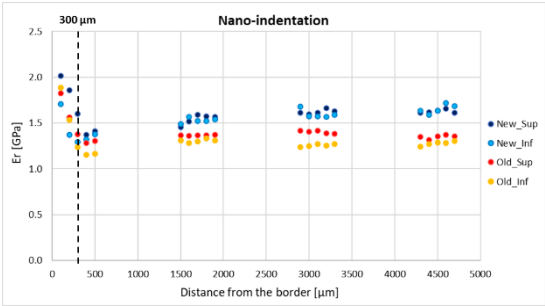


Figure 6: Behaviour of reduced modulus (E*) as a function of the distance from the border of the cross section. *New* refers to the virgin sample while *Old* refers to the compressed sample.

Especially, the values of elastic modulus of the bulk of the resin (distance from the border > 300 µm) were found to be statistically different ($p < 0.008$) from the values of elastic modulus of the external portion of the sample (distance from the border < 300 µm).

## 3.2. *In vitro vs. In silico*

Figure 7 and Figure 8 show the comparison between the Force – Displacement curves obtained from *in vitro* and *in silico* analyses of the mandibular and maxillary setup, respectively.

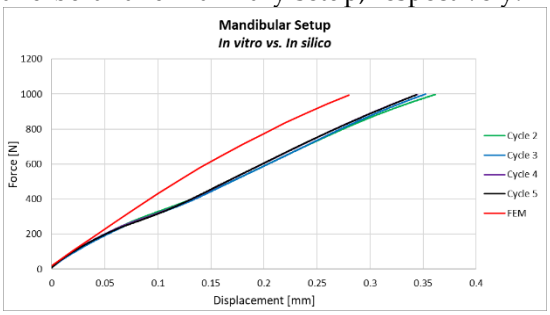


Figure 7: Force – Displacement curves obtained from *in vitro* and *in silico* analysis of mandibular setup.

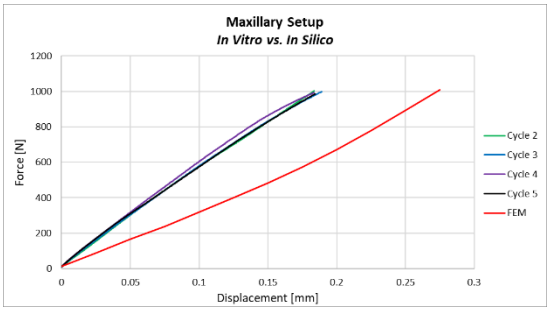


Figure 8: Force – Displacement curves obtained from *in vitro* and *in silico* analysis for maxillary setup.

For both cases, the nonlinear behaviour of the FEM curves is due to the elastoplastic properties implemented for the resin. In fact, considering the distribution of Von Mises Stresses on the bone phantom components, some areas were found to sustain stresses higher than the yield stress, causing plastic deformation. This is valid for both mandibular component (Figure 9) and for maxillary component (Figure 10).

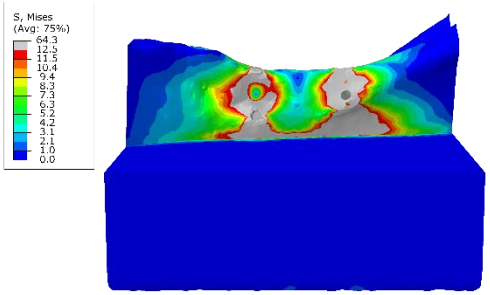


Figure 9: Distribution of Von Mises Stress on mandibular bone phantom. Grey areas are subjected to plastic deformation.

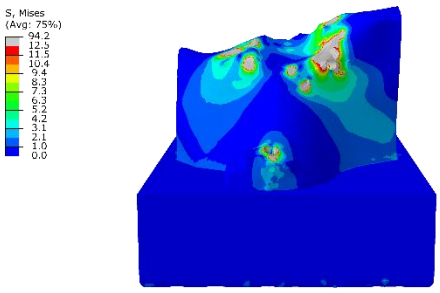


Figure 10: Distribution of Von Mises Stress on maxillary bone phantom. Grey areas are subjected to plastic deformation.

The mandibular implant and maxillary implants, instead, did not show any relevant yielded area. Comparing Force – Displacement curves, computational setup showed an overestimation of the measured force for displacement larger than 0.04 mm. In fact, for displacement belonging to the range [0.04; 0.12] mm, a variation of *in vitro* curve's slope provokes a gap between the forces measured by the two analyses. In this range, computational force revealed a maximum overestimation of 38.4%. Anyway, considering the overall stiffness of the setup, the behaviour of the last portion of the numerical curve is quite similar to the one obtained in vitro (error < 6%). Then, comparing Force – Displacement curves of the maxillary setup, the computational model showed an underestimation of the measured forces with a mean error of 48.6%. The overall stiffness of the experimental setup is always higher than the stiffness measured *in silico*. In the range of [0 – 0.04] mm of displacement, the measured mismatch is about 52.6% while, in the range of [0.135 – 0,180] mm the mismatch decreased at 26.1%.

## 4. Conclusions

The designed setups performed well during experimental tests of both mandibular and maxillary subperiosteal implants. All the auxiliary components were easy to assemble, cost effective and their material allows to reuse them for future analyses. Of course, to perform a more accurate and statistically relevant experimental analysis, a higher number of samples of the same implant type should be considered. Focusing on the computational model, all the software used to implement the same experimental setup fulfill their goal. The positioning of each component, the loading and constraining implementation did not show any issues. However, the comparison between *in vitro* and *in silico* analyses highlighted some critical aspects that should be improved. First of all, since the computational response of the bone phantom showed the presence of yielded zones, a more detailed analysis of both constitutive properties and time-dependent properties of the resin should be performed. Plus, regarding the resin, it could be interesting to understand its traction response. Then, the effect of the screws must be assessed. In fact, these elements are positioned manually during *in silico* analysis, and it is difficult to predict the exact position and inclination of each screw in the experimental bone phantom. For this reason, a sensitivity analysis of their inclination and their length should be performed to assess the variation of the overall stiffness. Among future developments, understanding the mechanical reliability of implants under a cyclic load with an experimental and a numerical approach, respectively, could be considered. In this way, the expected life years of subperiosteal implants can be assessed.

## 5. Bibliography

[1] L. J. Jin, I. B. Lamster, J. S. Greenspan, N. B. Pitts, C. Scully, and S. Warnakulasuriya, "Global burden of oral diseases: emerging concepts, management and interplay with systemic health," *Oral Dis.*, vol. 22, no. 7, pp. 609–619, 2016, doi: 10.1111/odi.12428.

[2] P. E. Petersen, D. Bourgeois, H. Ogawa, S. Estupinan-Day, and C. Ndiaye, "The global burden of oral diseases and risks to oral health," *Bull. World Health Organ.*, vol. 83, no. 9, pp. 661–669, 2005, doi: /S0042-96862005000900011.

[3] I. Petrovic *et al.*, "Oral rehabilitation of the cancer patient: a formidable challenge," vol. 117, no. 8, pp. 1729–1735, 2019, doi: 10.1002/jso.25075.ORAL.

[4] J. L. C. and R. A. Howell, "A classification of the edentulous jaws," no. 13, pp. 232–236, 1988.

[5] W. C. Oliver, G. M. Pharr, and I. Introduction, "An improved technique for determining hardness and elastic modulus using load and displacement sensing indentation experiments," 1992.